The Journal of Experimental Biology 214, 1017-1027

doi:10.1242/jeb.051227

RESEARCH ARTICLE

Burrow extension with a proboscis: mechanics of burrowing by the glycerid *Hemipodus simplex*

Elizabeth A. K. Murphy* and Kelly M. Dorgan†,‡

Department of Integrative Biology, University of California, 3060 VLSB #3140, Berkeley, CA 94720, USA

*Present address: Scripps Institution of Oceanography, 9500 Gilman Dr., La Jolla, CA 92037-0202, USA
†Present address: Department of Biology, University of Massachusetts, Amherst, MA 01003, USA
‡Author for correspondence (kdorgan@ucsd.edu)

Accepted 2 December 2010

SUMMARY

Burrowing marine infauna are morphologically diverse and ecologically important as ecosystem engineers. The polychaetes *Nereis virens* and *Cirriformia moorei* extend their burrows by crack propagation. *Nereis virens* does so by everting its pharynx and *C. moorei*, lacking an eversible pharynx or proboscis, uses its hydrostatic skeleton to expand its anterior. Both behaviors apply stress to the burrow wall that is amplified at the tip of the crack, which extends by fracture. That two species with such distinct morphologies and life histories both burrow by fracturing sediment suggests that this mechanism may be widespread among burrowers. We tested this hypothesis with the glycerid polychaete *Hemipodus simplex*, which has an eversible proboscis that is much longer and everts more rapidly than the pharynx of *N. virens*. When the proboscis is fully everted, the tip flares out wider than the rest of the proboscis, creating a shape and applying a stress distribution similar to that of *N. virens* and resulting in relatively large forces near the tip of the crack. These forces are larger than necessary to extend the crack by fracture and are surprisingly uncorrelated with the resulting stress amplification at the crack tip, which is also larger than necessary to extend the burrow by fracture. These large forces may plastically deform the mud, allowing the worm to build a semi-permanent burrow. Our results illustrate that similar mechanisms of burrowing are used by morphologically different burrowers.

Supplementary material available online at http://jeb.biologists.org/cgi/content/full/214/6/1017/DC1

Key words: burrowing, mud, sediment, *Hemipodus simplex*, biomechanics, fracture, gelatin, photoelastic stress analysis, stress intensity factor.

INTRODUCTION

Muddy marine sediments cover ~70% of the Earth's surface and provide habitat and food for a diversity of organisms. Burrowers are considered ecosystem engineers because of their role in bioturbation (the mixing of sediment grains and pore waters through ingestion, egestion and burrowing) (Meysman et al., 2006). This process affects the fate of pollutants, carbon and nutrient cycling, and contributes to benthic–pelagic coupling.

Marine muds are elastic solids through which worms extend burrows by fracture (Dorgan et al., 2005). Gelatin has similar mechanical properties and can be used as an analog material in studies of worms burrowing through this conveniently transparent medium (Dorgan et al., 2005). This mechanism of burrowing has been studied in two morphologically distinct species of polychaetes, *Nereis virens* Sars (Dorgan et al., 2007) and *Cirriformia moorei* Blake 1996 (Che and Dorgan, 2010). *Nereis virens* everts its pharynx to apply stress to the burrow walls; when enough stress is applied, and the stress is amplified sufficiently at the tip of the crack-shaped burrow, the resulting stress intensity factor (K_I) exceeds the critical stress intensity factor, or fracture toughness (K_{Ic}), and the burrow extends. The worm moves forward by undulation, moving its head from side to side, a behavior that also serves to extend the crack laterally to enlarge the burrow and reduce elastic compression on the worm from the surrounding sediment (or gelatin). *Nereis virens* can also extend its burrow by driving itself forward into the crack like a wedge rather than everting its pharynx (Dorgan et al., 2008). Both methods of burrow extension result in enough stress amplification at the crack tip to reach or exceed the fracture toughness of the medium through which the animal is moving. *Cirriformia moorei* uses its hydrostatic skeleton to dilate the anterior region, applying stresses to the burrow walls similar to those applied by an everted pharynx. The mechanics of burrow extension by fracture depend both on worm size (Che and Dorgan, 2010) and the material properties of the medium through which they burrow (Dorgan et al., 2008), and burrowing behaviors reflect these mechanical constraints. Specifically, the mechanics depend on the relative stiffness (E) and fracture toughness of the mud. In a material with high fracture toughness relative to stiffness, *N. virens* everted its pharynx to increase its thickness and bluntness. When fracture toughness was lower, worms instead moved their heads from side to side, effectively driving themselves forward like a thinner wedge and extending the crack laterally. Crack extension was modeled as stable, wedge-driven crack growth, and these behaviors were consistent with predictions from fracture mechanics theory of wedge shapes (Dorgan et al., 2008). The stress distribution along the crack walls is affected not only by the shape of the wedge, but also by the size of the wedge. As predicted, smaller worms exhibit behaviors analogous to those of worms in tougher materials; namely, increased relative thickness and bluntness (Che and Dorgan, 2010).

Considerable diversity in morphologies and sizes of burrowers exists, and how the mechanics of burrowing depend on morphologies

and behaviors has been largely unexplored. It is striking, however, in comparing the mechanics of burrowing by *N. virens* and *C. moorei*, that these morphologically different species apply very similar stresses with similar mechanical consequences. Extension of a narrow, pointy anterior region by *C. moorei* is analogous to side-to-side head movement by *N. virens* in that larger stresses are applied by the entire width of the body and focused to extend a narrower part of the crack. The crack is then extended laterally by side-to-side head movement or dilation of the anterior (to start a peristaltic wave) for *N. virens* and *C. moorei*, respectively. Without an understanding of fracture mechanics, similarity in the function of these two behaviors would likely be overlooked. Whereas *N. virens* uses its pharynx to apply a focused force near the tip of the crack where stresses contribute the most to the stress amplification at the crack tip, *C. moorei* dilates the anterior end of its body using its hydrostatic skeleton (Che and Dorgan, 2010). These analogous behaviors indicate that strategies such as applying large stresses close to the crack tip and focusing stresses exerted by a wide body to extend a narrower region of the crack may be utilized by other burrowers. Glycerid polychaetes have a long eversible proboscis and, like cirratulids, have a pointed head and move by peristalsis rather than undulation, making them an ideal organism for further examination of how morphology and behavior affect mechanisms of burrow extension by fracture.

Previous research on the proboscis has primarily focused on its use as a predatory feeding appendage (reviewed by Fauchald and Jumars, 1979; Rouse and Pleijel, 2001) – unsurprising given the large jaws at the end – but here we examine how it is used for burrowing. Some species of glycerids, e.g. *Glycera alba* Blegvad 1914, are known to build a complex network of permanent burrows (Ockelman and Vahl, 1970). We focused this study on *Hemipodus simplex* (Grube 1857), a lesser-studied species, but one that is locally abundant and burrows more readily in gelatin. Like other glycerids, *H. simplex* has a proboscis that is quite long, and has powerful jaws (Dales, 1962). We predicted that the forces and stress intensities exerted by *H. simplex* would be large on the basis of the assumption that they are predatory and need to move quickly through the sediment. These forces likely have a significant impact on sediment structure.

Despite the ecological importance of burrowing, the mechanism of burrowing by crack propagation has only recently been described (Dorgan et al., 2005; Dorgan et al., 2007). Here, we evaluate the role of the proboscis in burrowing by *H. simplex* in seawater gelatin, an analog for muddy sediments, and use photoelastic stress analysis to measure the forces exerted while burrowing (cf. Dorgan et al., 2007). To relate these forces to the mechanics of burrow extension by fracture, we also calculated the resulting stress intensity factors at the crack tip, predicting that larger forces would result in higher stress amplification and further crack extension. In addition to examining the role that force exerted by the proboscis plays in the mechanics of burrowing, we also evaluated whether proboscis eversion is necessary for burrow extension by glycerids, and examined mechanisms of burrowing without proboscis eversion. By studying a species with different morphology and behavior from previously studied worms, we can test our predictions that applying forces near the crack tip and extending a narrow crack relative to body width are strategies widely used to extend a burrow by fracture.

MATERIALS AND METHODS

Animals

Hemipodus simplex (mean ± s.d. 0.29±0.09 g wet mass; N=12 individuals) were collected from intertidal mudflats in Inverness and Bodega Bay, CA, USA, at low tide. Animals were kept in containers of mud under aerated seawater at 11°C until use in experiments.

Gelatin as an analog for muddy sediments

Muds have been shown to fail by fracture under relatively small forces applied on the spatial and temporal scales of burrowers (Johnson et al., 2002). Bubbles in both muddy sediments and seawater gelatin grow by fracture and have similar aspect ratios (Johnson et al., 2002). These aspect ratios depend on the ratios of the fracture toughness to the stiffness (K_{Ic}/E), which are similar in muds and gelatin, so we assume a similar dependence in the extension of an animal's crack-shaped burrow (e.g. Dorgan et al., 2005; Dorgan et al., 2007; Dorgan et al., 2008). This similarity may be due to gel-like mucopolymers that fill the pore spaces of muds (Watling, 1988) and dominate their bulk material properties (K.M.D., unpublished data).

Measurement of material properties

Because aquarium walls affect the stiffness of gelatin (cf. Dorgan et al., 2007; Dorgan et al., 2008), we measured E for the tanks ($0.14\times0.14\times0.20$ m) used in our experiments. Previously measured values of K_{Ic} (Dorgan et al., 2008) do not depend on tank size. An Instron 5544 material tester (Instron, Norwood, MA, USA) was used to measure force and displacement as a 6-mm-diameter sphere attached to a probe was lowered onto the surface of the gelatin at 0.5 mm s^{-1}. Stiffness relates stress (the force per area) to strain (the displacement normalized to original length), but the rigid aquarium walls prohibit calculation of stiffness from a simple linear relationship. Instead, the finite element modeling program franc2d (Cornell Fracture Group) was used to calculate a stiffness of 4131 Pa from a measured force of 0.033 N and a displacement of 3 mm, following methods described by Dorgan et al. (Dorgan et al., 2008).

Experimental setup

To analyze burrowing mechanics and kinematics, *H. simplex* was filmed burrowing in gelatin (Fig. 1). Lateral view video segments were used to measure the shape of the worm over several burrowing cycles, from which the stress intensity factor was calculated, following methods of Dorgan et al. (Dorgan et al., 2008). In addition, photoelastic stress analysis was used to visualize stress fields around the worm (Fig. 2) and measure the forces exerted by the everted proboscis (Dorgan et al., 2007).

Gelatin was made using powdered, food-grade gelatin (www.bulkfoods.com) and artificial seawater (Instant Ocean, Aquarium Systems, Inc., Mentor, OH, USA). A high-concentration mixture of seawater and gelatin was boiled, and then additional artificial seawater was added to reach a concentration of 28.35 g l^{-1} seawater. Liquid gelatin was poured into a 3.5 l glass aquarium and cooled overnight. Experiments were conducted in a cold room at 11°C. The aquarium containing gelatin was placed between a light table and a camera. The light table and the camera were covered by circular polarizing filters with opposing polarizations. The polarizing filters were lined up so that initially no light passed through the camera's filter. When a force is applied to the gelatin, a birefringent material, the light reorients in directions of maximal and minimal stress. The reoriented light passes through the camera's filter and shows up as a light area in monochrome video (Fig. 2B). The area of the resulting light patch (Fig. 2C) is proportional to the force (Dorgan et al., 2007).

The experimental setup (Fig. 1) comprised a Smartlight 5000 photographic light table (Just Normlicht, Weilheim/Teck, Germany) covered by a right-handed circular polarizing filter (3M HNCP 37%

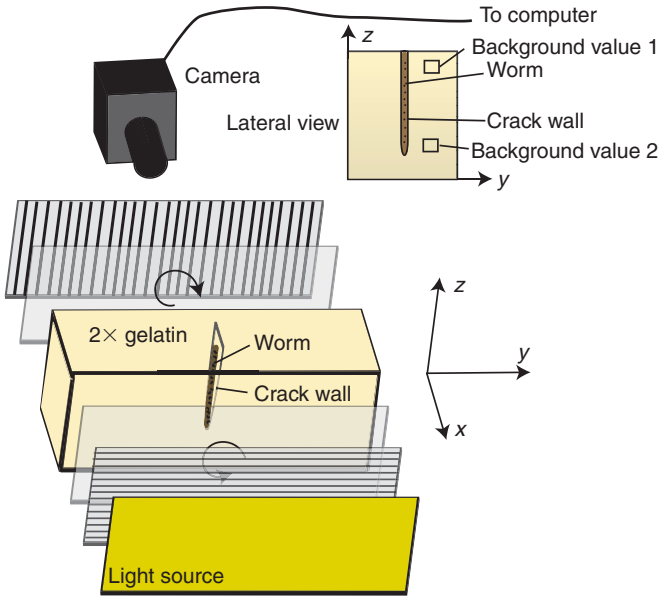

Fig. 1. Scheme of experimental setup. The aquarium (beige block) is placed between the light table (yellow block) and the camera, which was primarily used to record the lateral view of the worm, as shown. The *z*-direction is defined along the length of the worm, here shown as oriented downward in the aquarium. Background values used for force measurements are indicated. Between the light table and the aquarium is a right-handed circular polarizing filter with a left-handed circular polarizing filter between the aquarium and the camera. The circular polarizing filter is shown here as a linear polarizing filter with a quarter wave retarder; actual filters combine the two components. Filters on the far side of the cameras completely covered the light tables with no other light passing through, and the filters on the camera side were attached to the lenses. The camera was run from a computer with LabView software.

R.H. S-10×0.030 inches, Edmond Optics, Barrington, NJ, USA). In front of the light table was the aquarium of seawater-gelatin. A CCD videocamera (Basler A622f, Exton, PA, USA) with a 6× close-focus zoom lens (Edmund Optics #52-274) opposed the light table to record in lateral view images of the worm (defined as the *y*–*z* plane) at 7.5 frames s^{-1}. On the lens was a 52-mm, left-handed (standard) circular polarizing filter. Videos were recorded and analyzed using LabView software (version 7.1.1, National Instruments, Austin, TX, USA). A crack perpendicular to the camera was started with forceps, and a worm was placed in the crack. If it failed to burrow, or started burrowing and then stopped for a long period, it was gently prodded with a pipette. The macro lenses have a fixed focal distance, so the camera or the tank was moved to keep the distance between worm and camera constant. Our original setup (cf. Dorgan et al., 2007) used two cameras and two light tables at 90 deg angles, allowing dorsal and lateral video to be recorded at the same time. *Hemipodus simplex*, however, moves too quickly and unpredictably for adjusting both cameras to be feasible, so we used only one camera and one light table.

Video analysis for kinematics

For video to be used in analysis, the plane of the worm's crack had to be perpendicular to the field of view of the camera, and the tank was rotated to ensure a lateral view. If the worm was twisted, the video sequence was not used. Video was also rejected if the worm was oriented at an angle greater than 30 deg towards or away from the camera; when body stresses align with the stress from the proboscis, the area of the light region increases, leading to overestimation of forces. To limit wall effects, we rejected video segments in which the worm was ≤0.02 m from the aquarium wall. Videos were also rejected if they were not in focus. This approach eliminated video that was difficult to analyze and ensured constant distance between the worm and the camera for accurate measurements of worm body shapes and areas of the lighted regions.

Segments of video that showed the worm extending its burrow and met the above criteria were analyzed to calculate velocities of the worm and its proboscis eversion (supplementary material Movie 1). First, coordinates of the anterior tip of the worm's proboscis and the head were tracked throughout a burrowing cycle (using LabView). Second, we took multiple measurements of proboscis length; because the body and proboscis were not always straight, we determined the worm's body axis to account for curvature. For every frame, lines were drawn at regular intervals across the width of the worm, from the anterior tip along the worm's body (up to eight measurements) and along the proboscis (up to 12 measurements, depending on how far the proboscis was everted in each frame). The midpoints of each line were calculated using LabView to determine the body axis. Proboscis length was

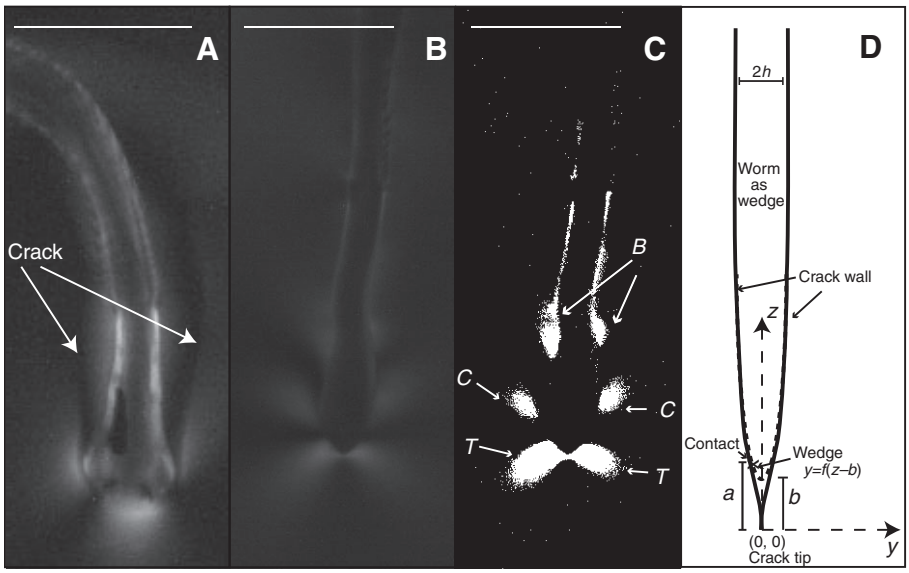

Fig. 2. Video frame of an everted *Hemipodus simplex* proboscis. (A) Dorsal view, with visible crack walls. (B) Lateral view of a different proboscis eversion and corresponding thresholded image (C). In C, the small upper patches of light posterior of the proboscis result from body stress (*B*). The light patches at the anterior end of the proboscis result from tensile stresses at the crack tip (*T*), and middle patches result from compressive stress (*C*) from the force of pharynx eversion and are the only pixels included in force calculations. (D) Scheme of the worm as a wedge of profile *f*(*z*–*b*) indicating the half-thickness (*h*) and distances from the crack tip to the point of contact (*a*) and from the crack tip to the anterior end of the worm (*b*) used in Eqns 1 and 2. Scale bars, 0.005 m.

determined by fitting a curve through the coordinates of the head, each midpoint and the anterior tip of the proboscis using MATLAB (MathWorks, Natick, MA, USA). Third, instantaneous velocity was calculated as the difference in proboscis length between a frame and the one just prior to it, divided by seconds per frame. Fourth, the distance traveled in an eversion cycle was calculated by fitting a curve through the anterior positions of the worm over the time of an eversion in each frame. Crack extension was determined as the maximum distance traveled in an eversion cycle. These kinematic data were obtained for 14 worms, with one to four eversions per worm.

Calculation of stress intensity factors

The stress intensity factor (K_I) was calculated from the measured worm thicknesses at each frame in the eversion cycle using MATLAB. From the lengths of lines used to measure proboscis length, thicknesses at up to 20 (for a fully everted proboscis) and at least eight (no eversion) points along the length of the worm were interpolated to obtain a smooth curve using a cubic spline function. Because the length of the worm visible in the field of view varied, the thickness of the posterior of the worm (the mean of the posterior two data points) was extended to a length of 0.02 m for consistency in further calculations. From the profile of the worm [$f(z–b)$], K_I was calculated by simultaneously solving two equations:

$$K_I = \frac{E\sqrt{2a}}{2\sqrt{\pi}\,(1-\nu^2)} \int_a^\infty \frac{f'(z-b)}{\sqrt{z(z-a)}}\,\mathrm{d}z,\ a > b \text{ (Sih, 1973)}, \quad (1)$$

$$K_I = \frac{E}{\sqrt{2\pi a}\,(1-\nu^2)} \left(h - \int_a^\infty f'(z-b)\sqrt{\frac{z-a}{z}}\,\mathrm{d}z \right) \text{ (Barenblatt, 1962)}, \quad (2)$$

described in detail by Dorgan et al. (Dorgan et al., 2008) and Che and Dorgan (Che and Dorgan, 2010) (Fig. 2D). Because a, the distance between the tip of the crack and the anterior-most contact of the worm with the crack walls, cannot be seen in video, two equations were needed to solve for the two unknowns, K_I and a, simultaneously. The distance between the crack tip and the anterior tip of the worm (b) is assumed to be the difference between the position of the anterior of the worm in a frame and its furthest position in previous frames. The worm's half thickness far from the anterior (h) is the mean of the two most posterior measurements, extrapolated to a length of 0.02 m. The slope of the worm's body [$f'(z–b)$] is calculated from thicknesses along the length (z-axis) of the worm. The stress intensity factor depends on the stiffness, or elastic modulus, [E (Pa)] and Poisson's ratio [ν (dimensionless)], which are both mechanical properties of the sediment or gelatin. To solve the two equations, an initially small value of a was incremented until the two values of K_I agreed to within 2 Pa m$^{0.5}$. Stress intensity factors were calculated for 11 worms for one to four eversions per worm.

Force measurements

Forces exerted by a worm's proboscis while burrowing were measured using photoelastic stress analysis, following the methods of Dorgan et al. (Dorgan et al., 2007). Before worms were introduced, each tank of gelatin was calibrated to relate the area of the light field to forces applied by test tubes of known mass (0.12–0.46 g) resting on the surface in the middle of the tank. Small plastic test tubes of the same size and style were used with tops cut off at different places to give different masses. Known volumes of water (0.1–0.2 ml) were added to the test tubes so the total masses being used for calibration ranged from 0.12 to 0.66 g. The relationship between force and area of the light region depends on the area of contact (Dorgan et al., 2007), so test tubes were chosen to match the contact area of the proboscis. The test tubes gave a diameter of contact with the surface of the gelatin of 0.0014–0.0024 m, depending on mass, and this was close to the length of the everted proboscis segment exerting a force on the gelatin (0.0009–0.0013 m). An image of a ruler was used to convert pixels to meters for each video. The zoom and aperture of the camera lens were set before calibrating and were not changed throughout the trial.

To generate a calibration curve, an image was captured with Measurement Automation Explorer (National Instruments) for each test tube and water combination and analyzed using LabView to determine the number of pixels with values above (lighter than) a threshold value determined separately for each tank. A light intensity gradient at the surface of the gelatin (due to stress caused by shrinking as water evaporates from the surface) was digitally removed by subtracting an image taken without a test tube. A background pixel value was added back to the image to obtain a background with the original intensity without surface noise. The background pixel value was a mean of pixel values in an undisturbed dark region near the top of the aquarium just below the stress field from the test tube, and was constant for all images used in a calibration (background value 1 in Fig. 1). The threshold value was chosen to be low enough for the stress fields on both sides of the worm's everted proboscis to show up, but high enough so that only the stress field from the test tube was light, and none of the surrounding area. A linear regression between the number of pixels of the stress field (dependent variable) and the force exerted by the weight of the test tube on the surface of the gelatin was used to convert pixels to forces. The stress field around a force on the surface is similar to that around a force exerted by a worm against its burrow wall (Dorgan et al., 2007).

For videos of each eversion cycle that fit the previously mentioned criteria, forces were calculated from the area of the stress field around the worm. The frame showing the largest stress field was estimated visually, and this frame, along with two or three frames before and after, was analyzed. The threshold value from the calibration was adapted for each worm to compensate for an observed gradient in background light intensity with depth in the tank, less extreme than the surface gradient, but amounting to a difference of 1 to 4 pixels between the surface and depth of the worm. A background value was calculated in the same manner as in the calibration, from pixels in an undisturbed dark region at the same depth as the worm's pharynx (background value 2 in Fig. 1). The difference between this background value and the background value used for calibration was then subtracted from the threshold value used for calibration, and this new number was used as the threshold for measuring the forces. In most thresholded images, three distinct lighted regions were visible on each side of the burrow wall, consistent with stress distributions around the pharynx of *N. virens* (Dorgan et al., 2007). On each side of the worm's everted proboscis were compressional stresses (C), with anterior stress fields resulting from tension at the crack tip (T) and posterior stress fields resulting from internal pressure in the proximal region of the proboscis (B) (Fig. 2B,C).

We included only the compressive stresses around the proboscis in our measurements (labeled 'C' in Fig. 2C), and the two sides were analyzed separately because a separate force was applied to each crack wall. The forces on both sides of the worm were averaged, and the maximum mean force was selected for each eversion. Forces were calculated for eight worms, with one to three eversions per worm. Because forces were small and measurement required the lateral view to be much more precisely aligned than for K_I, forces could not be determined for every worm.

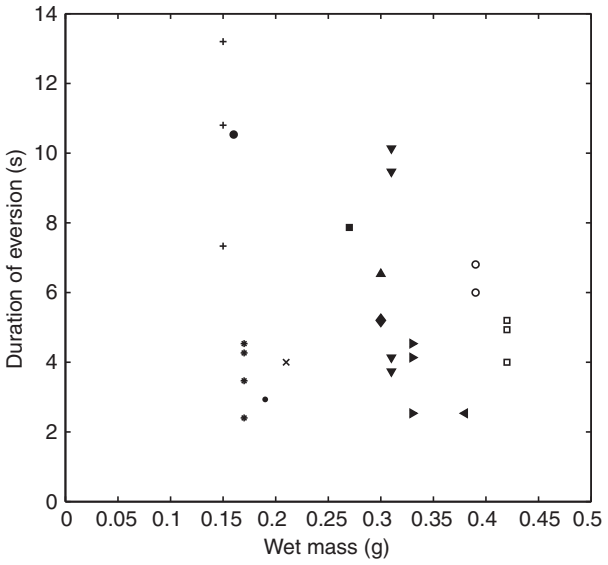

Fig. 3. Scatterplot of the duration of eversions of each replicate. Different symbols are used for each *H. simplex* individual, with each symbol indicating one eversion event.

RESULTS

Video analysis of burrowing kinematics

All worms observed everted their proboscises (supplementary material Movies 1, 2) to extend the burrows, but two worms were also observed extending their burrows by dilating their anterior end and then pushing their narrow head forward. We refer to this behavior as 'surging'. More worms may have exhibited this behavior and been overlooked, as we were primarily interested in proboscis eversion, and difficulty in adjusting the camera and tank to maintain a constant distance while worms moved quickly and erratically resulted in considerable periods of unusable video. After the burrow is extended using either method, the worm moves forward by peristalsis. Worms often paused in their forward movement for long periods and were prodded gently to encourage them to resume burrowing.

Burrowing events were highly variable, both for individual worms and among all worms studied. Eversions were erratic in direction and inconsistent in frequency. Proboscises did not always extend fully, and the duration of eversions had a large range, from 2.4 to 13.2 s (Fig. 3, Table 1). Maximal instantaneous proboscis velocity always occurred within the first frame or two of the beginning of the eversion, and reached as high as 0.036 m s^{-1} (Table 1). Crack extension was less variable and was much larger for proboscis eversion than surging; 0.006±0.001 and 0.0005±0.0001 m, respectively (means ± s.d.; Table 1).

For most videos, the field of view was too small or the worm's movement too inconsistent to capture successive cycles of proboscis eversion and movement without the camera being moved. For two worms, however, the camera was zoomed out

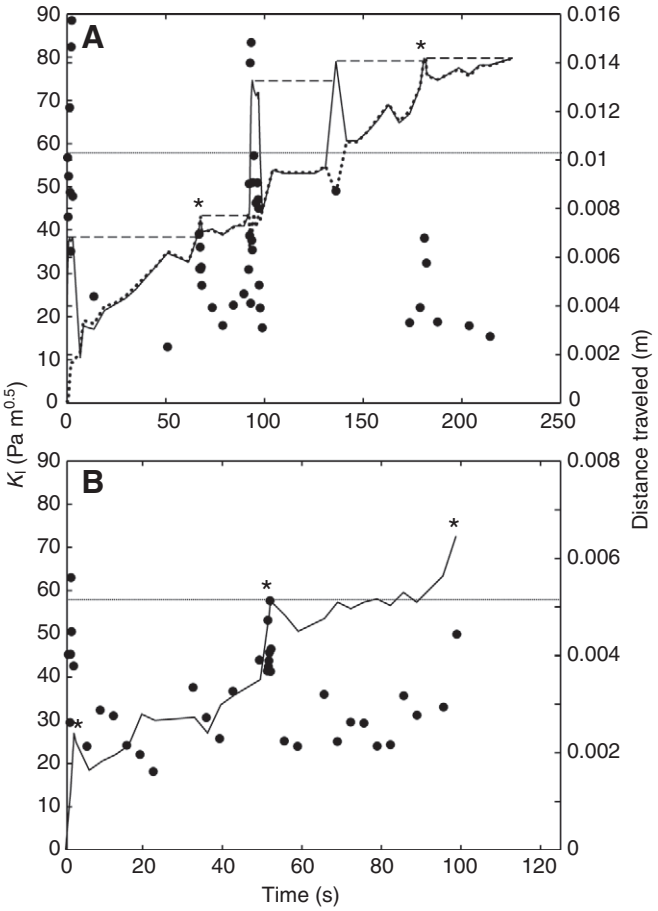

Fig. 4. Distances traveled by two representative worms (*H. simplex*) and corresponding stress intensity factors (K_I). Fracture toughness, or critical stress intensity factor (K_{Ic}), of gelatin is shown as a horizontal line at K_{Ic}=58 Pa $m^{0.5}$. (A) Distance traveled by a worm that both everted its proboscis and extended the crack by surging. The position of the anterior tip of the proboscis (solid line) and head (dotted line) over time is shown, with the corresponding stress intensity factor (filled circles). The crack is extended five times over the duration of burrowing, shown in the graph by horizontal dashed lines connecting a peak (extent of crack growth) to the next time the worm reaches that position and begins to extend the crack again. Two surges are marked with asterisks. Eversions are distinguished from surges by a clear difference between the position of the head and anterior tip of the worm's proboscis; during a surge the positions are identical as the proboscis is not everted. In addition, eversions extend the crack much further than surges. (B) Distance traveled by anterior tip of a different worm while burrowing without everting its proboscis (solid line) and corresponding stress intensity values (filled circles). The three surges are marked with asterisks. The second surge event is analyzed in Fig. 5B.

Table 1. Kinematic data for *Hemipodus simplex*

	Mean	Min.	Max.
Length of eversion (s)	5.9±2.5 (*N*=14)	2.4	13.2
Max. instantaneous proboscis velocity (m s^{-1})	0.014±0.006 (*N*=10)	0.008	0.036
Length of proboscis at max. K_I /max. length during eversion (dimensionless)	0.89±0.10 (*N*=12)	0.31	1
Max. length of proboscis (m)	0.006±0.001 (*N*=13)	0.004	0.009
Crack extension; eversions (m)	0.006±0.001 (*N*=13)	0.004	0.008
Crack extension; surges (m)	0.0005±0.0001 (*N*=2)	0.0003	0.0006

Values are means ± s.d. *N*=number of individual worms; replicate eversions for an individual were averaged.

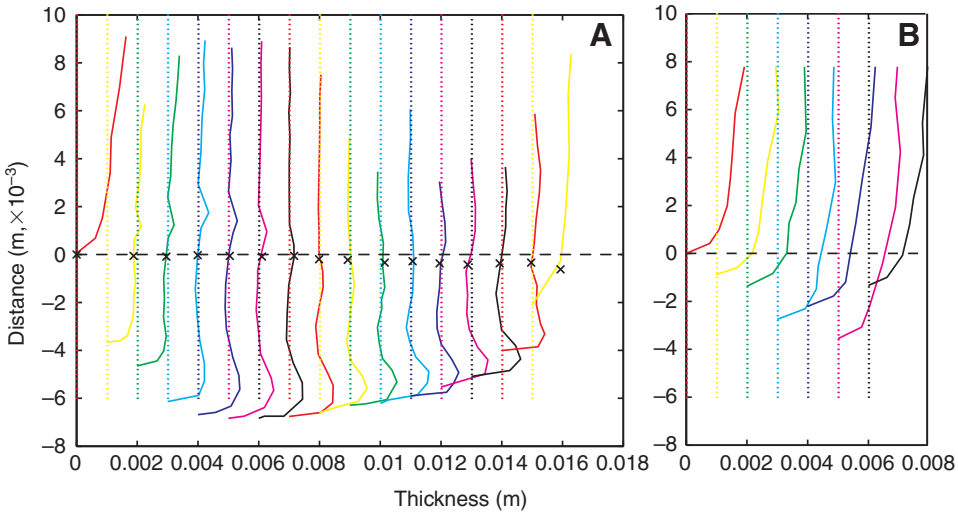

Fig. 5. Waterfall plots showing the lateral profile of a representative worm (*H. simplex*) extending its burrow by (A) everting its proboscis and (B) surging. Half thicknesses are solid lines and the corresponding midlines are dotted lines of the same color. Each frame (0.13 s) is staggered by 0.001 m. The position of the anterior end of the worm is set at 0 in the first frame, and the distances traveled by the proboscis and the head are shown as negative positions. In the first profiles, the proboscis was not everted. x, the position of the head in each frame in A. In B, the head is always at the tip of the worm.

enough to follow several eversions, for which the distances traveled over time by the worms' head and proboscis were measured (Fig. 4). One worm (Fig. 4A) exhibited periods of burrowing with both proboscis eversions and surges. Another worm burrowed without everting its proboscis (Fig. 4B). This burrowing sequence included three surge events. Compared with surge events, stress intensity factors were higher and crack extension was farther during proboscis eversion (Fig. 4A, Table 1). During eversions, the stress intensity factor reached a maximum slightly before the proboscis was fully everted, at 89±10% of its maximum length, although this, too, was highly variable, ranging from 31 to 100% (Table 1).

The lateral shape of a worm changes over eversion and surge cycles (Fig. 5). When the worm burrows without everting, its head remains pointed (Fig. 5B), as opposed to flaring out during a proboscis eversion. When a worm everts its proboscis, it extends the crack farther than when it surges (Fig. 5, Table 1). Worms flare out their proboscises while everted (Fig. 2A,B). As the proboscis becomes fully everted, it becomes wider at the distal end than near the worm's head (Fig. 2B). This flaring can be seen from a dorsal view as well (Fig. 2A, supplementary material Movies 1, 2).

Worms were often observed pulsing their proboscises when fully everted, especially during longer eversions (Fig. 6). During a longer eversion, the proboscis remained everted for several seconds and

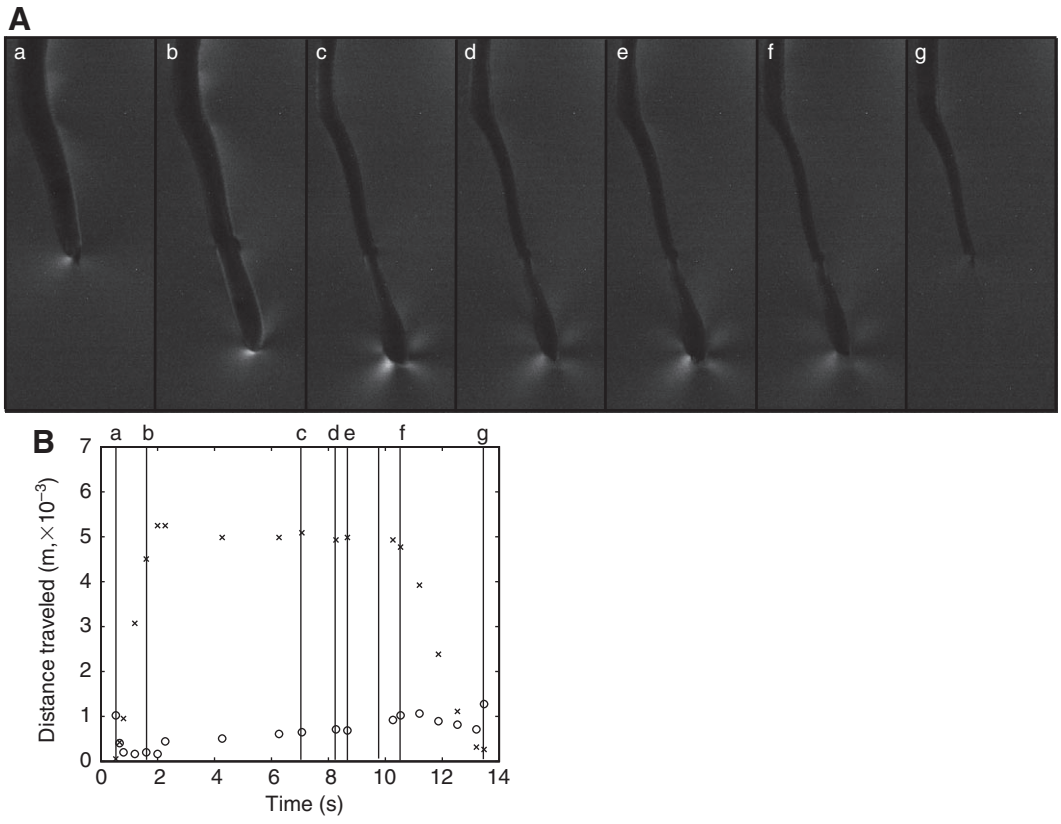

Fig. 6. (A) Sequence of lateral images from a long proboscis eversion in *H. simplex*. Images correspond to marked points in B. (B) Distance traveled by head (o) and proboscis (x) over time during one eversion cycle.

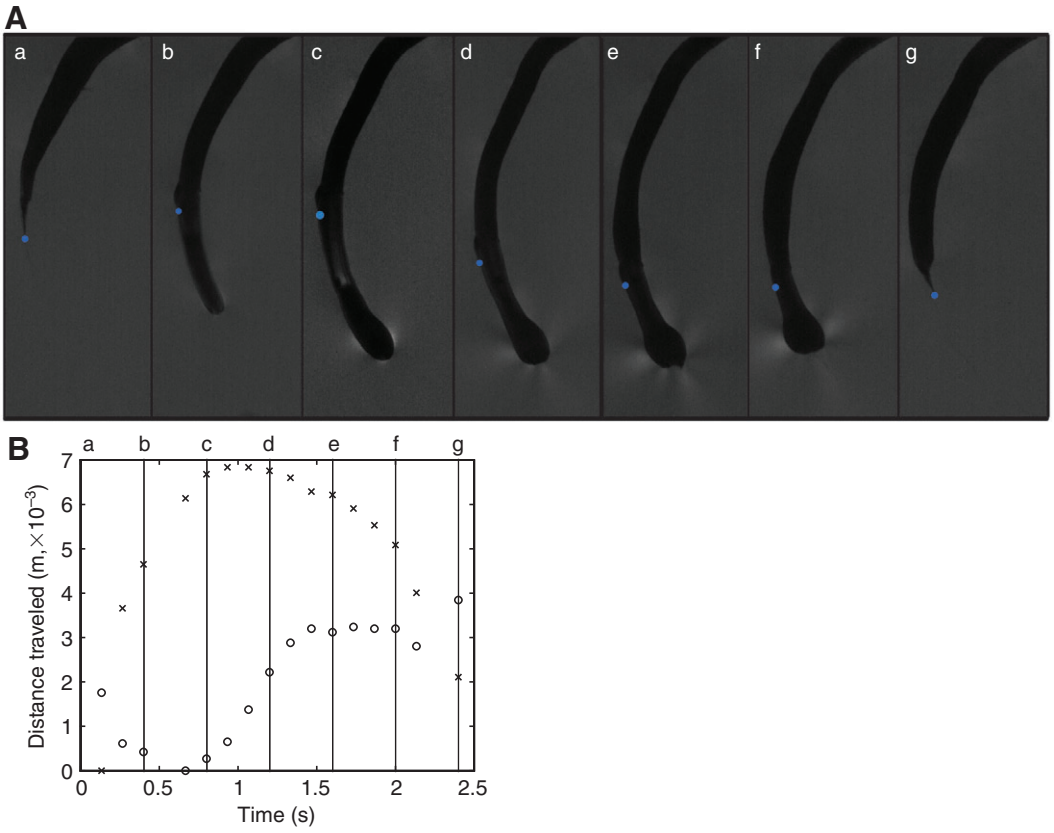

Fig. 7. (A) Sequence of lateral images from a short proboscis eversion in *H. simplex*. Images correspond to marked times in B. A blue circle marks the position of the head. The jaws are visible in e. (B) Distance traveled by head (o) and proboscis (x) over time during one eversion cycle.

pulsed repeatedly, while the jaws opened and closed. During shorter eversions, the proboscis expanded and then was retracted without pulsing (Fig. 7).

Stress intensity factors

During burrow extension, the stress intensity factor at the crack tip reached or exceeded the critical value for proboscis eversion (Table 2, Fig. 4A) and was close for surging (Table 3, Fig. 4B). Maximum stress intensity showed no correlation with wet mass of the worms (r^2=0.0001, P=0.98).

Table 2. Force and stress intensity measurements for eversions by individual worms (*H. simplex*)

Wet mass (g)	Force (×10^{-3} N)	K_I (Pa m$^{0.5}$)
n.d.	2.2±0.6 (*n*=3)	79.3±18.0 (*n*=3)
0.15	n.d.	65.7±6.3 (*n*=3)
0.17	n.d.	93.2±10.5 (*n*=4)
0.19	3.0 (*n*=1)	105.1 (*n*=1)
0.21	n.d.	75.5 (*n*=1)
0.27	2.1 (*n*=1)	n.d.
0.30	n.d.	74.7 (*n*=1)
0.30	2.0 (*n*=1)	104.8 (*n*=1)
0.31	n.d.	71.1±4.5 (*n*=4)
0.33	n.d.	84.6±5.1 (*n*=3)
0.38	2.4 (*n*=1)	57.5 (*n*=1)
0.39	2.2±0.2 (*n*=2)	101.0±15.5 (*n*=2)
0.42	2.4±0.02 (*n*=3)	88.9±7.2 (*n*=3)
Mean of all worms		
0.29±0.09 (*N*=12)	2.3±0.4 (*N*=7)	83.4±15.5 (*N*=12)

Values are means ± s.d. *n*, number of replicate eversions for each individual; *N*, number of individuals; n.d., not determined.

Force measurements

In images of stress fields around the everted proboscis, force is clearly exerted on the crack walls by a small area of the proboscis, 16.0±2.9% of the total length (*N*=4 individuals; Fig. 2C). Force also showed no correlation with wet mass of the worms (r^2=0.17, P=0.42), and no correlation was found between stress intensity and force (r^2=0.0032, P=0.92; Fig. 8).

DISCUSSION

Burrowing behavior and mechanics

Hemipodus simplex extends its burrow both by everting its proboscis, exerting a large force on the crack walls, and by surging, a behavior in which the worm dilates its anterior end and pushes itself forward into the crack. These events correspond with a greatly increased stress intensity factor compared with when the worm is moving into an already created crack (Fig. 4). Both of these mechanisms result in a stress intensity value close to or exceeding the critical stress intensity value of the gelatin and extension of the worm's crack-shaped burrow. Of the two worms that we analyzed surging, one produced a stress intensity factor equal to the critical value whereas the other was slightly lower. This lower value is not surprising, as

Table 3. Stress intensity measurements for surges by individual worms (*H. simplex*)

Wet mass (g)	K_I (Pa m$^{0.5}$)
0.3	53.9±7.8 (*n*=4)
n.d.	38.4±0.3 (*n*=2)
Mean of all worms	46.1±10.9 (*N*=2)

Values are means ± s.d. *n*, number of replicate surges for each individual; *N*, number of individuals; n.d., not determined.

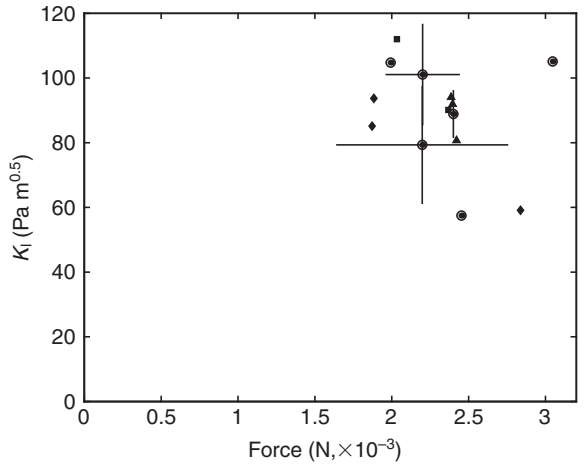

Fig. 8. There is no statistically significant correlation between maximum force and maximum stress intensity (K_I) (r^2=0.0032, P=0.92) in *H. simplex*. Double circles indicate means for an individual with error bars indicating ±s.d. for that individual; points without error bars had only one replicate. Other symbols indicate individual eversions, with all eversions by one individual shown with the same symbol.

the worms have pointed heads and wider bodies and our model for calculating K_I assumes constant width of the crack and the stresses applied; additional stress amplification likely occurs from the difference in width between the worm and the narrower new crack area (cf. Dorgan et al., 2008).

The flared shape of the proboscis has been observed in a scanning electron microscope image of *G. alba*, likely from proboscis eversion during preservation of the worm [fig. 10D in Tzetlin and Purschke (Tzetlin and Purschke, 2005)]. We observed a similar flared shape when *H. simplex* burrows in gelatin, and this shape enables the worm to exert a localized force with the tip of its proboscis, close to the crack tip. From fracture mechanics theory (Eqns 1, 2), stress nearer the crack tip contributes more to the stress intensity. In addition to increasing the stress intensity factor, flaring the tip of the proboscis allows the worm to exploit the constraint of the crack tip to exert a larger dorso-ventral force on the crack walls. Dorgan et al. showed that *N. virens* makes its anterior thicker and blunter when burrowing through a medium with relatively high fracture toughness to stiffness ratio (Dorgan et al., 2008). This thicker, blunter wedge shape results in a larger K_I.

When *H. simplex* everted its proboscis to burrow, the forces applied and the resulting stress intensity factors did not correlate, contrary to our expectations (Fig. 8). We expected larger forces to result in larger stress intensity factors, causing the crack to extend farther in front of the worm. Although we were only able to measure both force and stress intensity for six worms, a small sample size, the absence of even a trend raised questions about our assumptions, specifically to what extent the force exerted by the tip of the proboscis contributes to stress intensity at the crack tip. To address this question, we used finite element modeling to calculate stress intensity for a representative eversion. We then used the model to determine the relative contributions of the distal region of the proboscis exerting the force (p_a), the proximal region of the proboscis (p_b), around which no distinct stress field could be seen, and the body of the worm (b) to the stress intensity factor (Fig. 9).

To assess the contribution of measured forces to stress intensity factors, we applied stresses calculated from measured forces from the everted proboscis to the wall of a two-dimensional plane strain

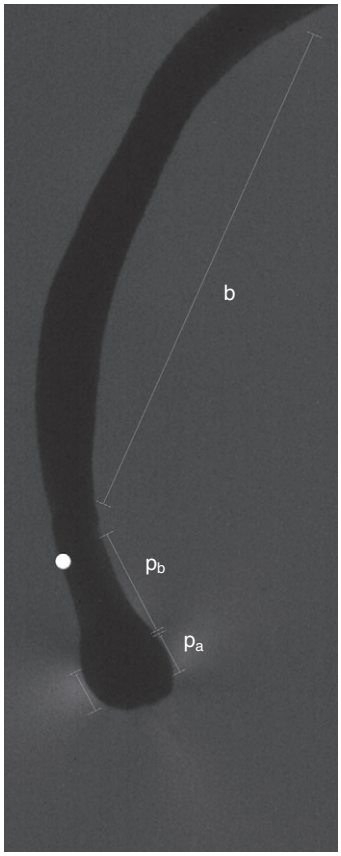

Fig. 9. *H. simplex* with an everted proboscis showing components of the total stress intensity during proboscis eversion. Distances over which stress is applied by the flared part of the everted proboscis (p_a), the distal part of the proboscis (p_b) and the body of the worm (b) are shown. The white circle indicates the tip of the worm's head.

model of the crack (lateral view of the worm) using the finite element modeling program franc2d (Cornell Fracture Group) (cf. Dorgan et al., 2007). To match the stress distribution around the proboscis of a representative worm visualized using photoelastic stress analysis, we applied no stress to the anterior-most 7% of the crack surface, stress calculated from measured forces (2300 Pa) to the next 14% of the surface and lower stress along the rest of the proboscis and body. For our representative modeled proboscis (6.9 mm long), the anterior 0.5 mm exerted no stress, 1.0 mm exerted the measured force and the remaining 5.4 mm exerted less stress. Because these stresses were much smaller and were not focused, the forces could not be measured using photoelastic analysis. Stresses instead were estimated, by trial and error, to be those that resulted in displacements matching the shape of the worm. To obtain body and proboscis thicknesses matching our representative worm, 500 Pa was applied along the proboscis proximal to the force, and stress linearly decreasing from 150 to 100 Pa was applied along the body (5 cm length).

The stress intensity factor for our modeled representative worm was 95 Pa m$^{0.5}$, close to those calculated using the wedge equation (Table 2). To determine the relative contributions of stresses from the focused force at the tip of the proboscis, the remainder of the proboscis and the body to the total calculated stress intensity factor, we removed the stress from each region and recalculated the stress intensity factor. Because the stress intensity factor is a measure of stress amplification under linear elastic conditions, the principle of

superposition applies, and stress intensity factors can be summed from stresses that sum to the total stress distribution (Anderson, 2005). By repeating this procedure for each of the three regions – the body (b), the proximal region of the proboscis (p_b) and the distal region exerting the force (p_a) (Fig. 9) – we calculated the contribution of each region to the total K_I (Table 4). We then used these numbers to evaluate whether the force applied near the tip of the crack is necessary to extend the crack by fracture and calculated the minimum force necessary for the stress intensity factor to reach the critical value. The combined contribution of the body and the proximal region of the proboscis to K_I is 43 Pa m$^{0.5}$, a considerable portion of that needed to reach a K_{Ic} of 58 Pa m$^{0.5}$ for gelatin. The worm exerted a force of 0.003 N, which alone results in a K_I of 52 Pa m$^{0.5}$, much higher than the 15 Pa m$^{0.5}$ needed in addition to the 43 Pa m$^{0.5}$ applied by the body and posterior region of the probosicis to reach the critical stress intensity factor. This force is 3.4 times larger than the 0.00087 N necessary to increase the total K_I to the critical stress intensity value and extend the burrow by fracture. In terms of stress applied to the crack wall, a force of 0.00087 N corresponds to a stress of 680 Pa, not much larger than the stress of 500 Pa needed to obtain the shape of the rest of the proboscis. Because the force generates only slightly more than 50% of the total K_I, and K_I exceeds K_{Ic} considerably, it is less surprising that the stress intensity and force values are not correlated. This suggests that the large forces and resulting stress intensity factors likely serve a purpose beyond extending the crack, although it is possible that the worm is extending its burrow out in front of the proboscis tip. More likely, these large forces are applied in creating a permanent burrow, a process for which gelatin is not an appropriate analog material. Many glycerids create permanent burrows, and although data are lacking for *H. simplex*, we have observed that when *H. simplex* moves through the mud, a cylindrical burrow is left behind.

A stress intensity factor exceeding K_I is mechanically impossible; rather, the crack extends until K_I drops to K_{Ic}. Using this finite element model, crack extension beyond the tip of the everted proboscis, difficult to see in our videos, can be estimated. The modeled crack was extended incrementally by 0.0005 m until the calculated stress intensity factor dropped to that for gelatin, K_{Ic}=58 Pa m$^{0.5}$ (cf. Dorgan et al., 2008). Once the stress intensity factor drops to the critical value, crack growth stops. Extending the crack 0.0025 m in front of the tip of the proboscis resulted in a drop in K_I to a K_{Ic} of 58 Pa m$^{0.5}$. Extending the crack out in front of the proboscis would enable the worm to move farther for each proboscis eversion, and could also provide some advantage in capturing prey.

Forces in natural sediments

On the basis of the assumption that the shape of the worm is constant whether the worm is burrowing in gelatin or sediment, the forces applied by worms in different media are proportional to the stiffnesses of those media (Dorgan et al., 2007). Body shape depends on the ratio of the fracture toughness to the stiffness (K_{Ic}/E): in relatively tougher materials, body shape is thicker and blunter. Dorgan et al. measured thicknesses of *N. virens* burrowing in gels with K_{Ic}/E ratios spanning a range occurring in natural sediments and found significantly thicker bodies (normalized to body width to account for size differences, resulting in a dimensionless value) in the toughest material, 0.92±0.10, compared with 0.68±0.08 for a relatively stiff material (Dorgan et al., 2008). This variability in K_{Ic}/E occurs in natural sediments, indicating that the forces exerted by worms also vary considerably and depend on the stiffness and fracture toughness. Nonetheless, calculation of approximate force applied by a worm in natural sediments can be done by simply multiplying the force measured in gelatin by the ratio of mud stiffness to gelatin stiffness. Dorgan et al. (Dorgan et al., 2007) calculated the differences in forces in natural sediments from those in gelatin using finite element modeling to account for differences in stiffness as well as hypothesized differences in Poisson's ratio (ν), a measure of compressibility. No measurements of Poisson's ratio for natural sediments were made, but assuming that sediments are more compressible than gelatin, ν decreased from 0.45 for gelatin to 0.30 for sediment, which decreased the predicted force by 17% (Dorgan et al., 2007). This difference in forces based on hypothesized differences in compressibility is less than the variability resulting from body shapes, which increase by 35% from a stiff to a tough medium (or decrease by 26% from a tough to a stiff medium).

Because the model used by Dorgan et al. (Dorgan et al., 2007) was linear, we can use a simpler method and calculate forces from the ratio of mud stiffness to gelatin stiffness, here 27 kPa/4.1 kPa. A mean force of 2.3×10^{-3} N in gelatin equates to a force of 0.015 N in sediment. For comparison with measured forces by *N. virens*, it is necessary to include the difference in Poisson's ratio, which decreased the force by an estimated 17%, here to 0.0125 N. This is much smaller than the forces exerted by *N. virens*, but the worms were much smaller, 0.285±0.089 g for *H. simplex* compared with 8.2±3.9 g for *N. virens*.

Comparison with other burrowers

Both *N. virens* and *H. simplex* use eversible mouthparts to extend their burrows by fracture. Relative to body length, *H. simplex* has a much longer proboscis than *N. virens*, but because *H. simplex* flares the end of the proboscis, the stress distribution along the burrow wall is remarkably similar between the two species. Similar expansion near the crack tip is achieved in the cirratulid *C. moorei* through its hydrostatic skeleton and dilation of the anterior region, which also initiates a peristaltic wave (Che and Dorgan, 2010). The surging behavior observed in *H. simplex* is very similar to movement by *C. moorei*, which burrows by peristalsis without everting its mouthparts. Both species have pointed anterior ends that extend a crack narrower than the posterior of the body and then dilate the body to expand the crack laterally.

Hemipodus simplex uses peristalsis to move forward into the extended crack whereas *N. virens* undulates its body. Undulation,

Table 4. Stress intensity factors contributed by different parts of eversion in *H. simplex*, the maximum total stress intensity generated by the eversion, the critical stress intensity factor, the K_I contributed by the shape of the worm (b+p_b)

Contributing factor	K_I (Pa m$^{0.5}$)	K_{Ic} (Pa m$^{0.5}$)	Applied stress (Pa)
Dilated region of proboscis (p_a)	52		2300
Posterior region of proboscis (p_b)	30		500
Body (b)	13		100–150
Total K_I	95	58	
b+p_b	43		

or side-to-side head movement, by *N. virens* also serves to extend the crack laterally away from the body to relieve elastic compressive stresses. *Hemipodus simplex* does not exhibit this behavior, but its proboscis tip expands laterally as well as dorso-ventrally. This lateral expansion appears to be analogous to the side-to-side head movement of *N. virens* in extending the crack laterally away from the worm. *Cirriformia moorei* achieves lateral crack extension at the same time as it applies a dorsoventral force by dilating the anterior end.

A much larger but morphologically similar glycerid, *Glycera dibranchiata*, also burrows by everting its long proboscis. In order to explore the effects of size on burrowing behaviors and forces, we observed this larger worm burrowing in gelatin. *Glycera dibranchiata* is ~30 times the mass of the *H. simplex* used here (10.05 g for *G. dibranchiata* compared with 0.285±0.089 g for *H. simplex*). Like *H. simplex*, *G. dibranchiata* burrows by everting its mouthparts, and it, too, flares out the tip of its proboscis, which contains a large set of jaws. This worm has more difficulty burrowing in gelatin, taking longer to begin burrowing and stopping more frequently, but when it everts its proboscis it either makes a large crack that extends quite far in front of the proboscis or it leaves a highly disrupted region of gelatin rather than a single crack, seeming to shatter the gelatin. It is possible that either the magnitude of force or the rate of eversion that can be applied to the crack walls determine whether a single crack extends or branches, resulting in gelatin shattering. Even for the smaller *H. simplex*, the velocity of the proboscis at the beginning of the eversion is high, and proboscis eversion by glycerids likely produces one of the fastest rates of fracture that muddy marine sediments experience. Time dependence of fracture has not been studied in sediments or gelatin, so the observed shattering of gelatin does not necessarily represent the effect on natural sediments. The potential for crack branching and shattering of natural sediments as a mechanism for creating a permanent burrow, or as a way to break through prey burrow defenses (such as burrow linings), is intriguing. It is also possible that rapid proboscis eversion creates enough fluid motion to break force arches *via* liquefaction in granular sediment, which *G. dibranchiata* is known to move through. These hypotheses are not mutually exclusive, and certainly merit further study.

In preliminary experiments, we calculated the force exerted by *G. dibranchiata* using the same methods as those for *H. simplex*. The force was 0.039 N, ~20 times the mean force exerted by *H. simplex* (0.0023±0.0004 N).

Comparison of forces between different sizes of individuals of different species is challenging. Although no studies have measured the size dependence of forces by polychaetes, large earthworms, *Lumbricus terrestris*, exerting radial forces against rigid force transducers, exert forces smaller than predicted by a 2/3 power law; rather, the relationship between force (F) and mass (m) was $F=0.32m^{0.43}$ (Quillin, 2000). This relationship is consistent with predictions from fracture mechanics theory that small worms need to exert relatively more stress to reach the critical stress intensity factor and extend the burrow by fracture. We compared forces exerted by these two polychaetes, 0.0125 and 0.16 N for *H. simplex* and *N. virens*, respectively [using the calculation for *H. simplex* including the decrease in Poisson's ratio, following methods from Dorgan et al. (Dorgan et al., 2007)], with radial forces by earthworms of similar size, 0.19 and 0.79 N. Forces exerted by earthworms are much larger, but those forces were measured against rigid walls, enabling the earthworms to exert larger forces, rather than against a deformable medium, in which the magnitude of the force is limited by the displacement, or thickness, of the worm. In addition, earthworms live in soils that are often unsaturated, and they need to be able to maintain body shape against gravitational forces; a terrestrial lifestyle adds an additional energetic cost to animals with hydrostatic skeletons (K.M.D., unpublished data). Not only are the total forces larger for earthworms, but the difference in forces exerted by *H. simplex* and a small earthworm is greater than that between a small earthworm and *N. virens*, contrary to our expectations. Including the force exerted by *G. dibranchiata* (0.21 N following the same methods to convert from gelatin to mud), the range is even larger for polychaetes. In fact, fitting a power-law curve to our three data points (of questionable comparability, as they are from three different species) yields $F=0.01m^{1.3}$, an unrealistically high exponent. We expected large worms to exert relatively smaller forces than small worms, i.e. the power law to be closer to that found by Quillin (Quillin, 2000) for earthworms, and predatory glycerids to exert larger forces than other polychaetes. The data point for *N. virens* is not noticeably lower than that for *G. dibranchiata*, but rather seems to suggest that larger worms do indeed exert larger than expected forces. Measuring forces by small worms using photoelastic stress analysis is challenging, but there was unlikely to be enough error in measured forces for *H. simplex* to account for the large difference in forces between large and small worms. We suspect that the large forces are associated with permanent burrow creation; however, further research is clearly needed to elucidate the relationships among forces exerted and body size, and the impacts of these forces on sediments.

The burrowing behavior of *H. simplex* is consistent with fracture mechanics theory. The worm drives crack growth by making a wedge shape, and generates relatively large stress intensities by becoming a thick, blunt wedge. This is similar to behaviors exhibited by *C. moorei* and *N. virens* when they are burrowing through a tough medium. Burrowing by crack propagation appears to be a widespread and common method of locomoting through muddy sediments in polychaetes with diverse morphologies and behaviors. Descriptions of burrowing mechanisms by a diversity of burrowing organisms, such as clams, burrowing urchins and a variety of worms, are consistent with this mechanism of burrowing by crack propagation (Dorgan et al., 2006). This study broadens our understanding of burrowing mechanics in polychaetes by illustrating similarities among worms with different morphologies, and these similarities likely extend to other phyla as well.

ACKNOWLEDGEMENTS

We thank M. A. R. Koehl, Pete Jumars and an anonymous reviewer for helpful comments on the manuscript. This project was funded by NSF IOS grant no. 0642249 to M. A. R. Koehl, as well as the Virginia G. and Robert E. Gill Chair to M. A. R. Koehl and the Undergraduate Research Apprenticeship Program, University of California, Berkeley.

LIST OF SYMBOLS

a	distance from the tip of the crack to the point of contact between the anterior end of the worm and the crack wall
b	distance between the anterior end of the worm and the tip of the crack
B	body stress
C	compressional stress around the proboscis
E	modulus of elasticity (Pa)
h	half-thickness of a worm at a point far away from the anterior end
K_I	stress intensity (Pa m$^{0.5}$)
K_{Ic}	critical stress intensity factor (Pa m$^{0.5}$)
T	tensile stress at crack tip
ν	Poisson's ratio (dimensionless)

REFERENCES

Anderson, T. L. (2005). *Fracture Mechanics: Fundamentals and Applications*. Boca Raton, FL: CRC Press.

Barenblatt, G. (1962). The mathematical theory of equilibrium cracks in brittle fracture. In *Advances in Applied Mechanics*, Vol. 7 (ed. H. L. Dryden and T. von Karman), pp. 55-129. New York: Academic Press.

Che, J. and Dorgan, K. M. (2010). It's tough to be small: dependence of burrowing kinematics on body size. *J. Exp. Biol.* **213**, 1241-1250.

Dales, R. P. (1962). The polychaete stomodeum and the inter-relationships of the families of Polychaeta. *Proc. Zool. Soc. Lond.* **139**, 389-428.

Dorgan, K. M., Jumars, P. A., Johnson, B. D. and Boudreau, B. P. (2006). Macrofaunal burrowing: the medium is the message. *Oceanogr. Mar. Biol.* **44**, 85-121.

Dorgan, K. M., Jumars, P. A., Johnson, B. D., Boudreau, B. P. and Landis, E. (2005). Burrow elongation by crack propagation. *Nature* **433**, 475-475.

Dorgan, K. M., Arwade, S. R. and Jumars, P. A. (2007). Burrowing in marine muds by crack propagation: kinematics and forces. *J. Exp. Biol.* **210**, 4198-4212.

Dorgan, K. M., Arwade, S. R. and Jumars, P. A. (2008). Worms as wedges: effects of sediment mechanics on burrowing behavior. *J. Mar. Res.* **66**, 219-254.

Fauchald, K. and Jumars, P. A. (1979). The diet of worms: a study of polychaete feeding guilds. *Oceanogr. Mar. Biol. Annu. Rev.* **17**, 193-284.

Johnson, B. D., Boudreau, B. P., Gardiner, B. S. and Maass, R. (2002). Mechanical response of sediments to bubble growth. *Mar. Geol.* **187**, 347-364.

Meysman, F. J. R., Middelburg, J. J. and Heip, C. H. R. (2006). Bioturbation: a fresh look at Darwin's last idea. *Trends Ecol. Evol.* **21**, 688-695.

Ockelmann, K. W. and Vahl, O. (1970). On the biology of the polychaete, *Glycera alba*, especially its burrowing and feeding. *Ophelia* **8**, 275-294.

Quillin, K. J. (2000). Ontogenetic scaling of burrowing forces in the earthworm *Lumbricus terrestris*. *J. Exp. Biol.* **203**, 2757-2770.

Rouse, G. W. and Pleijel, F. (2001). *Polychaetes*. Oxford: Oxford University Press.

Sih, G. C. (1973). *Handbook Of Stress Intensity Factors: Stress Intensity Factor Solutions And Formulas For Reference*. Bethlehem, PA: Lehigh University.

Tzetlin, A. B. and Purschke, G. (2005). Pharynx and intestine. *Hydrobiologia* **535/536**, 199-225.

Watling, L. (1988). Small-scale features of marine sediments and their importance to the study of deposit feeding. *Mar. Ecol. Prog. Ser.* **47**, 135-144.